X-shaped space-time coherence in optical parametric generation

O. Jedrkiewicz,[1] M. Clerici,[1] A. Picozzi,[2] D. Faccio,[1] and P. Di Trapani[3,*]

[1]*CNISM and Department of Physics and Mathematics, Università dell'Insubria, Via Valleggio 11, 22100 Como, Italy*
[2]*Laboratoire de Physique de l'Université de Bourgogne, CNRS UMR 5027, Dijon, France*
[3]*Department of Quantum Electronics, Vilnius University, Sauletekio 9, LT 10222 Vilnius, Lithuania*

We study the spatiotemporal coherence properties of superfluorescence radiation generated in optical parametric amplification of quantum noise. We show that the angular dispersion properties of the spatiotemporal spectra, measured in different phase-matching conditions, lead to a clear *X*-shaped structure of the mutual correlation function of the radiation. Within a statistical picture, we interpret the generated superfluorescence as a stochastic "gas" of quasistationary modes characterized by a skewed correlation in the spatiotemporal domain, with characteristics similar to linear and nonlinear *X* waves not describable within a separable approach in space and time.

I. INTRODUCTION

Coherence is a key physical concept underlying the statistical properties of a large variety of fundamental phenomena, such as Bose-Einstein condensation, superfluid flows, superconductivity [1,2], laser light emission [3,4], hydrodynamic turbulent flows [5], or synchronization of biological rhythms [6]. In optics, which is the natural context to discuss this notion, the simplest manifestations of correlations in fluctuating electromagnetic fields are the well-known interference effects that arise when two light beams originating from the same source are superposed. The elementary concepts of spatial coherence were first introduced by Wolf in 1955 to characterize the statistical properties of partially incoherent light [3,4,7]. Conventionally, a light field is called coherent when there is a fixed phase relationship between the electric field values at different locations or at different times, within the chosen statistical ensemble. Therefore, spatial coherence refers to the ability of a field to interfere with a spatially shifted (but not delayed) region of the same field, whereas temporal coherence describes the similar ability to interfere with a delayed (but not spatially shifted) version of itself. The coherence time τ_c is conveniently measured by using a Michelson interferometer, leading to a longitudinal coherence length of the light defined as $\Delta l = c\tau_c$, c being the light speed in vacuum. The Young's interference experiment, on the other hand, gives information on the spatial coherence area σ_c of the radiation [3]. From these definitions, usually adopted in the case of a nearly plane, quasimonochromatic linearly polarized wave, follows the concept of coherence volume around a particular point of the field, which is described as the right-angle cylinder occupying a domain of volume $\Delta V = \sigma_c \Delta l$ [3]. The coherence volume appears then as a space–time factorizable quantity, which corroborates the general idea that a separable characterization of the spatial and temporal properties of coherence provides a convenient

description of fluctuating fields, as witnessed by common interferometric measures of coherence.

In fact a unified mathematical description of these notions of spatial and temporal coherence is provided by the mutual coherence function or autocorrelation function, permitting us, for instance, to evaluate the (partial) correlation that exhibits a wave field at two distinct points, or at the same point at different instants of time. This autocorrelation function characterizing a random fluctuating field is usually written as $\Gamma(\vec{r}_1, \vec{r}_2, t_1, t_2) = \langle V^*(\vec{r}_1, t_1) V(\vec{r}_2, t_2) \rangle_e$, where the average $\langle \cdots \rangle_e$ is intended to be made over an ensemble of different realizations of the field [3]. In particular when the field exhibits a stationary statistics, the mutual correlation function only depends on the time delay $\tau = t_1 - t_2$ and if the field statistics is also ergodic the ensemble average can be replaced by a time average. A complex degree of coherence is obtained by normalizing Γ, and usually, in the literature, the complex degrees of temporal and spatial coherence are obtained separately by setting $\vec{r}_1 = \vec{r}_2$ or $\tau = 0$, respectively. These provide information about the degree of correlation between two fields arriving in the same position but at two different instants separated by a time interval τ or between two fields arriving simultaneously in two different points [3,7]. In this paper the concept of stationarity will be readdressed within the context our experimental work, involving a pulsed radiation field.

Note for completeness that, whereas the traditional coherence theory considers only the lowest order field correlation function, Glauber's approach presented in 1963 [8] considers correlation functions of any order both in quantum theory and in classical theory and shows, in particular, that fields generated by conventional optical sources are coherent only at the lowest order. In fact, the most important difference with respect to the traditional approach is the introduction of a succession of correlation functions for the complex field strengths, where the *n*th order function expresses the correlation values of the fields at 2*n* different points in space and time (i.e., the intensity correlation, which is proportional to the joint probability of photodetection at *n* space-time points). The notion of complete coherence requires then that the field correlation functions satisfy an infinite succession of

---

*Permanent address: CNISM and Department of Physics and Mathematics, Università dell'Insubria, Via Valleggio 11, 22100 Como, Italy.

coherence conditions (see also Ref. [3], Chap. 12). In fact, for the purpose of our work, we will deal in this paper with first order coherence only, and with the diagnostic technique used to measure it in the full spatiotemporal domain.

In many fields of physics, common experimental measurements of coherence are usually aimed at providing a separate characterization of the spatial and temporal coherence properties of fluctuating phenomena. This is the case in optics for the study of the statistical (temporal) properties of laser radiation or of radiation emitted from different kinds of sources such as, for instance, thermal sources [9,10]. Astronomical interferometers are also typically used to study the degree of spatial correlation existing, over great areas, in the light reaching the Earth's surface from individual stars [9]. On the other hand, dynamical light scattering experiments (see, e.g., Refs. [11–13]) often evaluate field correlations in both the spatial and temporal domain. Nevertheless, regarding the notion of radiation coherence volume, we recently reported experimental evidence of a direct and complete space-time characterization of radiation coherence [14]. Precisely, we showed the existence of a state of *X*-shaped spatiotemporal coherence, i.e., a state in which coherence is neither spatial nor temporal, but skewed along specific spatiotemporal trajectories [15]. Such a peculiar coherent state results from the combined action of (spatial) diffraction, (temporal) dispersion, and nonlinearity. In this respect, we have pointed out that the emission process may be pictured as a stochastic generation of an ensemble of skewed correlated modes, the latter resembling nonlinear *X* waves, which are coherent localized structures recently discovered in various contexts [16–28].

Before going into detail, let us discuss the physical origin of *X* coherence from a different point of view. For this purpose, let us recall that emergence of coherence in the parametrically down-converted fields relies on the interplay between natural wave dispersion and the nonlinear parametric amplification. The term "dispersion" is used here in a broad sense and refers both to first order dispersion effects (i.e., spatial or temporal walk-off between the down-converted fields) as well as second-order dispersion effects (i.e., diffraction or group-velocity dispersion). When first- (second-) order dispersion effects dominate the interaction, it is known that the coherence time or length of the down-converted fields increases as $z^{1/2}$, ($z^{1/4}$), z being the propagation distance in the crystal. As a result, when second-order dispersion effects may be neglected, the coherence of the fields appears thanks to the feedback action caused by the walk-off between the waves. Let us stress, however, that in the presence of both a spatial and a temporal walk-off, the concept of walk-off is generalized to two dimensions and hence has a vector nature. In this case, coherence will be established in those skewed space-time directions in which spatial and temporal walk-off compensate each other, a property that was discussed in Ref. [15]. Because walk-off may be regarded as a first-order dispersive effect, this skewed coherent state is induced by walk-off in the same way as *X* coherence is induced by second-order dispersive effects. As a result, *X* coherence emerges along two specific spatiotemporal trajectories in which temporal dispersion and spatial diffraction compensate each other. This is illustrated in Fig. 1, which
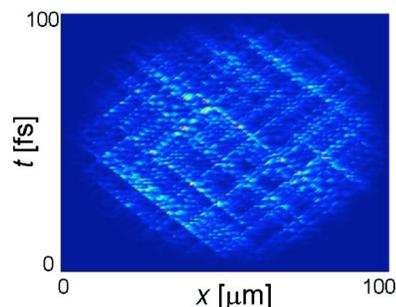

FIG. 1. (Color online) Numerical simulation showing the spatiotemporal intensity distribution of the down-converted signal field at the propagation distance $z=1$ mm with parameters corresponding to the conditions of the experiment reported in Sec. II B (the simulation has been performed in $(2+1)$ dimensions in the paraxial and slowly varying envelope approximation).

shows that the down-converted field has reached a peculiar state of coherence characterized by the presence of *X*-shaped lines of correlation, a peculiar feature that will be discussed in detail in Sec. III.

The aim of this paper is to extend the previous work [14] on the experimental observation of optical waves characterized by *X*-shaped spatiotemporal coherence, by presenting measurements and results. Through the analysis of several different experimental configurations, we prove the generality of the aforementioned property of the parametric down-conversion process. Consequences on the nature of the emitted field (e.g., mode structure, stationarity) are also discussed. With this work, we confirm that the dichotomous picture of spatial and temporal coherence fails to describe the coherence properties of a large variety of nonlinear wave systems. In Sec. II, we provide a complete and detailed description of the experiment for the direct characterization of such a nontrivial volume of coherence, realized from correlations measurements over the entire space-time domain, and in different experimental configurations. The experimental setup and the spectral method used for such a purpose is described in Sec. II A. In Sec. II B, we present measurements of the spatiotemporal correlation function in the case of parametric radiation generated by a type-I beta-barium-borate (BBO) crystal. We illustrate single-shot spectra recorded in different phase-matching configurations, together with the corresponding correlation function calculated by means of a spatiotemporal Fourier transform. In Sec. II C we comment on the quasistationarity of the spatiotemporal modes, which constitute, in our picture, the stochastic distribution of the near-field radiation. Experimental measurements of single-shot radiation generated within a lithium triborate crystal (LBO), and covering a different frequency range than that of the BBO, are then presented in Sec. II D. Section III is devoted to the theoretical and numerical model analyzed in 2D+1 dimensions. It provides further insight into the mechanism underlying the emergence of *X*-shaped spatiotemporal coherence. In Sec. IV, we describe in detail the interferometric measurement based on Young's experiment, corroborating the existence of skewed coherence. Finally a summary and the conclusions of our work are presented in Sec. V.

II. SPECTRAL MEASUREMENTS AND COHERENCE

It is worth noting that the nonlinear mechanism underlying the formation of the peculiar coherent states skewed in the spatiotemporal reference frame essentially relies on symmetry considerations associated with momentum and energy conservation laws, that is, the phase-matching conditions of the parametric amplification process [29]. A first extensive study of the spontaneous optical parametric process in nonlinear, anisotropic, and dispersive media, was presented by Giallorenzi and Tang in Ref. [30], where the tuning characteristics, beam divergence, and spectral properties of the emission for collinear and noncollinear interactions have been described in detail and illustrated with numerical examples. In fact, we shall see that the key feature of the emission spectrum that leads to an *X*-shaped spatiotemporal coherence is the angular dispersion (i.e., the dependence of the angle of the emitted radiation on the radiation wavelength), which is determined by phase matching, independently of the type of operation (degenerate or nondegenerate). For the sake of simplicity this can be illustrated by considering the basic process of parametric generation around degeneracy, in which a second harmonic (pump) beam, of frequency ω_2, parametrically amplifies quantum noise fluctuations in a spectral region around the fundamental harmonic frequency $\omega_1 = \omega_2/2$ [16,29]. By projecting the phase-matching condition along the longitudinal axis z of propagation, one has $\Delta k_z = k_{2,z}(\omega_2) - k_{1,z}(\omega_1 + \Omega) - k_{1,z}(\omega_1 - \Omega)$, where $\vec{k}_{1,2}$ represent the wave vectors of the beams and Ω a detuning of the signal frequency with respect to ω_1. Expanding then the dispersion relation $k_{1,z}(\omega_1 + \Omega)$ to second order in Ω and making use of the paraxial approximation, one readily obtains $\Delta k_z = K^2/k_1 - \Omega^2 k_1''$, where $K^2 = k_{1,x}^2 + k_{1,y}^2$ and $k_1'' = (\partial^2 k_1/\partial \omega^2)$. It becomes apparent that whenever a nonlinear material exhibits normal dispersion $k_1'' > 0$, preferential amplification ($\Delta k_z \simeq 0$) occurs for spatial and temporal frequencies lying along an *X*-shaped spectrum. Thus, if the crystal is oriented in such a way (with respect to the pump direction) that axial emission occurs at degeneracy (i.e., $K = 0$ for $\Omega = 0$), such an *X*-shaped spectrum is defined by the two symmetric lines $K = \pm \sqrt{k_1 k_1''}\Omega$. Note that the features characterizing simultaneous angle and wavelength one-beam noncritical phase matching have been studied numerically and theoretically by Lantz and co-workers in Ref. [31], clearly illustrating how the gain exhibits an *X*-shaped plateau at degeneracy. Actually, spatiotemporal emission spectra characterized by angular dispersion (independently of the spectral features around degeneracy) will be shown to witness the presence of a field featuring an *X*-shaped correlation function in the space-time domain, i.e., a coherence volume characterized by a nonfactorizable, spatiotemporal biconical (hourglass) shape.

The aim of the experiment is precisely the characterization of the coherence properties of the superfluorescence radiation generated by a quadratic $\chi^{(2)}$ nonlinear process of parametric amplification of vacuum field fluctuations. Two experimental configurations are considered: in the first case (a), the parametric radiation is generated in the visible range by a BBO crystal pumped by a ultraviolet laser pulse and in the second case (b) an LBO crystal is pumped by a visible green pulse, generating superfluorescence in the infrared region of the spectrum. In case (a), the pump pulse is given by a $T_p = 1$ ps duration, $\Delta\lambda_p = 0.1$ nm spectral bandwidth (centered at $\lambda_2 = 352$ nm), $D_p = 200$ μm diameter, $E_p = 80$ μJ energy (peak power $P = 80$ MW), transform-limited Gaussian pulse. It is generated by frequency tripling the output of a chirped pulse amplification Nd:glass laser (Twinkle, Light Conversion, Ltd.), operated at 2 Hz repetition rate. The pump pulse is injected into a 2-mm-long BBO crystal, cut for a type-I degenerate interaction at $\lambda_1 = 704$ nm. In case (b), a similar pump pulse (but centered at $\lambda_2 = 527$ nm), with $D_p = 1$ mm diameter, $E_p = 200$ μJ energy (peak power $P = 200$ MW) is generated by frequency doubling the output of the Nd:glass laser, and is injected into a 15 mm-long LBO crystal, temperature tunable and cut for type-I degenerate interaction at $\lambda_1 = 1055$ nm. In both cases, the parametric down-converted radiation is generated over a conical broadband spectrum, whose characteristics are determined by the phase-matching conditions and the parametric crystal gain bandwidth [32,33]. The study of coherence properties of the superfluorescence is based on the measurement of the radiation spectrum resolved both in angle and wavelength (or, equivalently, transverse momentum and frequency) as described in the following.

A. The spatiotemporal spectral diagnostics

The direct demonstration of the existence of a nontrivial coherence volume shape (e.g., skewed in the spatiotemporal domain), has been achieved by means of an experimental technique that allows us to record the spatiotemporal spectrum of each single optical wave packet generated by the nonlinear crystal from one laser pump pulse. More precisely, the spectrum $\mathcal{S}(\theta, \lambda)$ of the spontaneously generated signal is analyzed in both the spatial and temporal domains, i.e., it is resolved in vertical angle $\theta \simeq K/k_1$ and in wavelength λ ($\omega_1 + \Omega = 2\pi c/\lambda$). For this purpose, the entrance slit of an imaging spectrometer (Oriel Instruments, MS260i) constituted by two toroidal mirrors (M_1 and M_2) and a dispersive grating G, is placed in the focal plane of a lens L ($f = 75$ mm) that collects the far-field signal of the radiation. This setting allows different vertical-angle components of the impinging radiation to enter the slit at different vertical positions. Note that the first measurements of far-field signal wavelength dependence on angle with respect to the pump direction were performed in 1968 by Budin *et al.* [34], in the regime of noncollinear phase matching, and were shown to be in accordance with the theoretical prediction. Our technique is also similar to that of Lantz *et al.* already used to show the features of a *X*-shaped (θ, λ) spectrum issued from $\chi^{(2)}$ amplification of a broadband source at degeneracy in a type-I crystal [35]. Moreover this diagnostic technique has been recently applied in many other contexts, where the retrieval of such spectra in both the spatial and the temporal domains has proved to be very useful for the understanding of the wave packets nonlinear dynamics [22,25,36,37].

In this work, the spectrum $\mathcal{S}(\theta, \lambda)$ is acquired by a high dynamic range (16-bit) CCD camera (Andor, EEV 40–11), placed in the spectrometer imaging plane, and a laser-
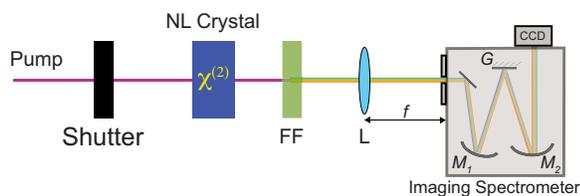
FIG. 2. (Color online) Schematic setup of the experimental apparatus. The pump after the nonlinear (NL) crystal is eliminated by means of filters denoted by FF (corresponding, respectively, to one interference filter centered at 352 nm for the BBO measurements, and to two broadband filters centered at 527 nm for the LBO measurements).

synchronized shutter permits single-shot acquisition of the radiation generated by a single laser pulse. During the data analysis, a calibration of the measured spectrum is performed by taking into account the CCD quantum efficiency curve as a function of the wavelength. A simplified scheme of the experimental apparatus used for the diagnostic is shown in Fig. 2.

The coherence hidden in the radiation spectrum is revealed through the analysis of the spatiotemporal correlation function $\mathcal{C}(\xi,\tau)$, which is calculated by means of the space-time Fourier transform of the averaged spectrum $\langle \mathcal{S}(K,\Omega) \rangle$ [where $\mathcal{S}(K,\Omega)$ is obtained from the spectrometer output spectrum $\mathcal{S}(\theta,\lambda)$], by virtue of Wiener-Kintchine theorem [3,4]. In our experiment, the average over-realization $\langle \mathcal{S}(K,\Omega) \rangle$ is recorded from multiple shots on chip integration by keeping the shutter open for a suitable time interval. Before entering into the details of our experiment, let us note that the theorem of Wiener-Kintchine is commonly used in statistical physics for the derivation of the correlation function [4] in the spatial domain or in the temporal domain, for instance, in all those light scattering problems concerning the study of the structural properties of molecular solutions (i.e., of spatial distribution of scatterers), or the study of the molecular temporal dynamics (see, e.g., Refs. [11] and [12], respectively). As we shall see here below, we will use a generalized form of the Wiener-Kintchine theorem extended in the space-time domain, that allows us to study the complete spatiotemporal coherence in a way conceptually similar to what is usually performed in dynamic light scattering experiments (see, for instance, Ref. [13]).

B. Experimental results from a type-I BBO crystal

We present here the spectral measurements and the evaluation of the mutual correlation function of the field of superfluorescence generated from the BBO crystal pumped by the 352-nm, 1-ps laser pulse. Figure 3(a) illustrates a typical example of spatiotemporal signal spectrum $\mathcal{S}$ retrieved from a single pump pulse. In this particular case where the crystal has been tuned for collinear emission at degeneracy, it exhibits a very clear X-shaped structure, which indicates the emission of radiation at angles θ increasing with the frequency shift Ω, as previously anticipated by the linear relationship $K = \pm\sqrt{k_1 k_1''}\Omega$ (note that the system is characterized by radial symmetry with respect to the z axis). Spectra with
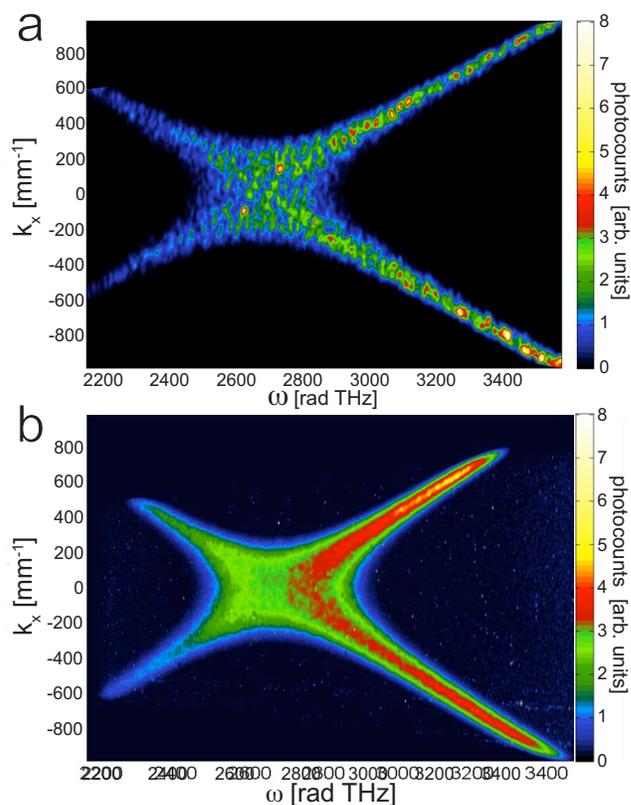

FIG. 3. (Color online) BBO Single shot spectrum (a), BBO integrated spectrum (b).

similar features, observed experimentally out of degeneracy in Ref. [34], and at degeneracy in the context of parametric amplification of a polychromatic image [35], have also been measured subsequently in many other works (see, for instance, Refs. [32,33]). They are now known to characterize X waves [16–26], which constitute the polychromatic generalization of diffraction-free Bessel beams [38]. However, in contrast to X waves, which are inherently coherent localized structures (i.e., characterized by smooth X spectra, see, for instance, Ref. [25]), here the spectrum exhibits a specklelike substructure reflecting the (partially) incoherent nature of the field. It is interesting to note the symmetry of the spatial intensity distribution of the speckles with respect to the collinear propagation direction ($\Omega = K = 0$), evidencing the far-field correlations existing between the phase-conjugated photon pairs (signal-idler) emitted in the PDC process and coupled through the phase-matching relations. We also mention that the symmetry of the speckles in angle has already been observed in far-field spatial patterns, together with evident classical signal-idler correlations of spatial fluctuations at a fixed wavelength (at degeneracy) [33]. These have also been studied numerically in Ref. [39]. On the other hand, the existence of such spatial correlations has also been predicted at the quantum level (see Ref. [40]), and subshot noise signal-idler intensity correlations have been recently measured around degeneracy in a type-II nonlinear crystal [41,42]. This incoherent specklelike pattern is a manifestation of the amplification of quantum vacuum field fluctuations. The structure of the speckles gives information about

the spatiotemporal gain profile of the spontaneous amplification process, and thus reflects the fact that the pump wave packet size is spatially and temporally finite (the speckles dimensions can be estimated in first approximation as $\delta\omega \sim T_p^{-1}, \delta k \sim D_p^{-1}$) [32]. On the other hand, the X-shaped envelope of the spectrum has to be related to the spatiotemporal modes of the superfluorescence radiation generated within the crystal and thus to their coherence volume structure.

It is worth noting that the spectrum is extended over very large temporal and spatial bandwidths ΔK and $\Delta\Omega$ ($\Delta\Omega$ almost spans the complete visible spectrum). If the radiation were analyzed by means of traditional techniques, one would be led to the erroneous conclusion that the field is spatially and temporally almost incoherent, since $\tau_c \sim 2\pi/\Delta\Omega \sim 5$ fs and $\Delta l \sim 2\pi/\Delta K \sim 3.5$ μm. However, in contrast to usual incoherent fields, whose spectra uniformly fill the space-time frequency domain (K, Ω), here the spectrum is sharply localized over a thin X-shaped surface. As we shall see later on (also in the case of degeneracy), the presence of skewed "arms" determined by the angular dispersion of the radiation is the key element characterizing the X-shaped space-time coherence. Figure 3(b) shows the result of the average of single shot spectra, obtained by integrating on the CCD the radiation fluence over 400 laser shots. In this way, we have assumed that, under stable laser conditions, each wave packet generated from a single pump pulse constitutes a distinct realization of the statistical ensemble and thus an equivalent replica of the system. In computing the average, the granularity gets evidently smoothed. The dependence on the vertical detection plane is removed owing to the radial symmetry with respect to the axis z.

In order to be rigorous, it is important to precise that given the short pulse duration and the small beam width of the signal field, the statistics of the signal cannot be assumed *a priori* homogenous and stationary. The autocorrelation $\mathcal{R} = \langle A_1(\vec{r}_{\perp 1}, t_1, z) A_1^*(\vec{r}_{\perp 2}, t_2, z)\rangle$ of the signal field results to be a function of both the "space-time distances" $\vec{\xi} = (\vec{r}_{\perp 1} - \vec{r}_{\perp 2})$, $\tau = (t_1 - t_2)$, as well the "space-time coordinates" $\vec{r}_{\perp 0} = \frac{1}{2}(\vec{r}_{\perp 1} + \vec{r}_{\perp 2})$, $t_0 = \frac{1}{2}(t_1 + t_2)$, where $\vec{r}_\perp = (x, y)$. Note that, as is usual in nonlinear optics, the variable t refers to the "retarded" time in a reference frame moving at the group velocity v_1 of the harmonic field. The spatiotemporal spectrum $\hat{\mathcal{R}} = \langle \hat{A}_1(\vec{K}_1, \Omega_1, z) \hat{A}_1^*(\vec{K}_2, \Omega_2, z)\rangle$ is thus linked to the autocorrelation by means of the generalized form of the Wiener-Khinchine theorem,

$$\mathcal{R}(\tau, \vec{\xi}, t_0, \vec{r}_{\perp 0}, z) = \int d\Omega \int d\vec{K} \int d\omega \int d\vec{k} \hat{\mathcal{R}}(\Omega, \vec{K}, \omega, \vec{k}, z)$$

$$\times \exp[i(\Omega\tau + \vec{K} \cdot \vec{\xi} + \omega t_0 + \vec{k} \cdot \vec{r}_{\perp 0})], \quad (1)$$

where $\Omega = \frac{1}{2}(\Omega_1 + \Omega_2)$, $\vec{K} = \frac{1}{2}(\vec{K}_1 + \vec{K}_2)$, $\omega = \Omega_1 - \Omega_2$, and $\vec{k} = \vec{K}_1 - \vec{K}_2$. However, the typical size of the speckles reported in the experiment is much smaller than the size of the X spectrum, which indicates that the signal statistics may be assumed to be quasihomogenous and quasistationary, as described by a straightforward spatiotemporal generalization of the Schell model of partially coherent light [3]. This also

reflects the fact that the spatiotemporal spectral bandwidth of the pump pulse is much narrower than the emission spectrum of the parametric fluorescence. The autocorrelation function may thus be factorized as $\hat{\mathcal{R}} \simeq \langle \mathcal{S}(\vec{K}, \Omega, z)\rangle \hat{I}(\vec{k}, \omega, z)$, where $\hat{I}$ takes into account the nonhomogenous and nonstationarity character of the statistics through the finite size of the speckles. In this respect, note that $\hat{I}(\vec{k}, \omega, z)$ tends to a Dirac's δ distribution in the limit of a homogenous and stationary statistics $\hat{I}(\vec{k}, \omega, z) = \delta^{(2)}(\vec{k})\delta(\omega)$. The correlation function $\mathcal{R} = \mathcal{C}(\vec{\xi}, \tau, z)I(\vec{r}_{\perp 0}, t_0, z)$ turns out to be the product of a stationary contribution $\mathcal{C}(\vec{\xi}, \tau, z)$, and a nonstationary contribution $I(\vec{r}_{\perp 0}, t_0, z)$, which simply corresponds to the space-time overall envelope of the signal intensity profile. $\mathcal{C}$ and I then, respectively, correspond to the space-time Fourier transform of $\langle \mathcal{S} \rangle$ and $\hat{I}$. Assuming the effect of the finite size of the pump negligible in our situation, all the information on the autocorrelation function can thus be extracted from the two-dimensional Fourier transform of the averaged spatiotemporal spectrum $\langle \mathcal{S}(\vec{K}, \Omega, z)\rangle$. Accordingly, this regime is analogous to that of a monochromatic plane wave, so that the averaged spectrum obtained from multiple shot acquisition "virtually" coincides with the averaged spectrum that would have been obtained if the pump were a continuous plane wave. In the same way, this regime is analogous to the one of dynamic light scattering experiments. Typically in the latter, the spectrum of the scattered radiation is detected at different angles and frequencies, leading to the so-called structure factor that is linked to the Fourier transform of the correlation. The result of these kinds of study is the retrieval of a full spatiotemporal correlation (see, e.g., Ref. [13]) in complete analogy to what we do here in our investigation of superfluorescence light. Clearly note that, contrary to our case, the physics involved in light scattering experiments only depends on linear response processes, and the origin of the detection of temporal spectral components is typically due to the temporal fluctuations of the scatterers (e.g., density fluctuations).

The result of the two-dimensional Fourier transform applied to our averaged spatiotemporal spectrum is illustrated in Fig. 4. Figure 4(a) shows the spatiotemporal correlation function $\mathcal{C}(\xi, \tau)$ of the signal field. The contour-plot representation is given in Fig. 4(b). As already noted [14], $\mathcal{C}(\xi, \tau)$ is also X shaped, indicating that two points in the field are correlated with each other only if their temporal delay τ and spatial distance ξ belong to such an X structure. As a result of the radial symmetry of the system, $\mathcal{C}$ only depends on the modulus $|\vec{\xi}|$, so that the X-shaped correlation function corresponds to a biconical shape in three dimensions. Interestingly, the size of the coherence volume evaluated at full width at half maximum (FWHM) of the correlation function leads to a transverse coherence length of 4 ± 1 μm and a coherence time of 6 ± 2 fs, respectively, in accordance with the estimation made by taking the inverse of the whole spatial (ΔK) and temporal $(\Delta\Omega)$ bandwidth, respectively, of the recorded spectrum. Nevertheless, it is only thanks to this diagnostic technique that the skewed extended arms of the spatiotemporal correlation can be experimentally observed,
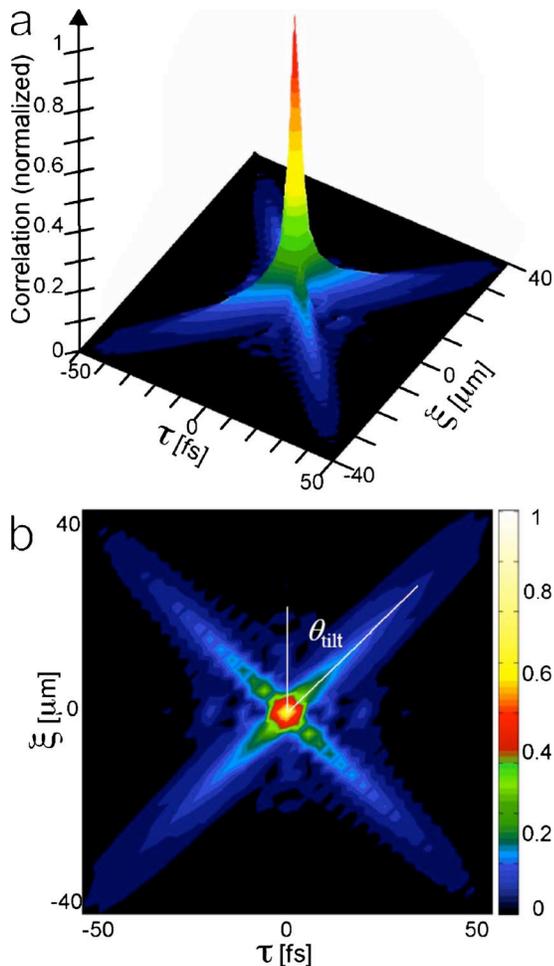
FIG. 4. (Color online) Spatiotemporal correlation function $\mathcal{C}(\xi, \tau)$ of the signal field from BBO (a), contour-plot representation (b).

FIG. 5. (Color online) Bidimensional FT of the single shot spectrum from BBO (a), contour-plot representation (b).

confirming also the nonfactorizability of the mutual coherence function investigated.

In the following we would like to illustrate the result of the application of the bidimensional spatiotemporal Fourier transform to a single-shot spectrum recorded by the CCD. Wiener-Kintchine theorem cannot be applied in this case, because such a single-shot spectrum constitutes a single realization of the statistical ensemble. Nevertheless we have observed that with this diagnostic technique it is still possible to extract qualitative information about the shape and structure of the correlation. Figures 5(a) and 5(b) show in logarithmic scale the results retrieved from the Fourier transform of the single-shot spectrum presented in Fig. 3(a). On the top of a noisy bell-shaped background (existing as a consequence of the fine specklelike structure of the spectrum), an X-shaped pattern can be identified, and the contour-plot representation clearly allows us to define the skewness of the correlation arms. An estimation of the FWHM of the peak of this structure leads to a rough estimation of the spatial and temporal dimensions of the coherence volume, these appearing to be slightly larger (but of the same order of magnitude) as those obtained from Fig. 4(b). This is due to the presence of the quantum noise fluctuations, which in the latter case
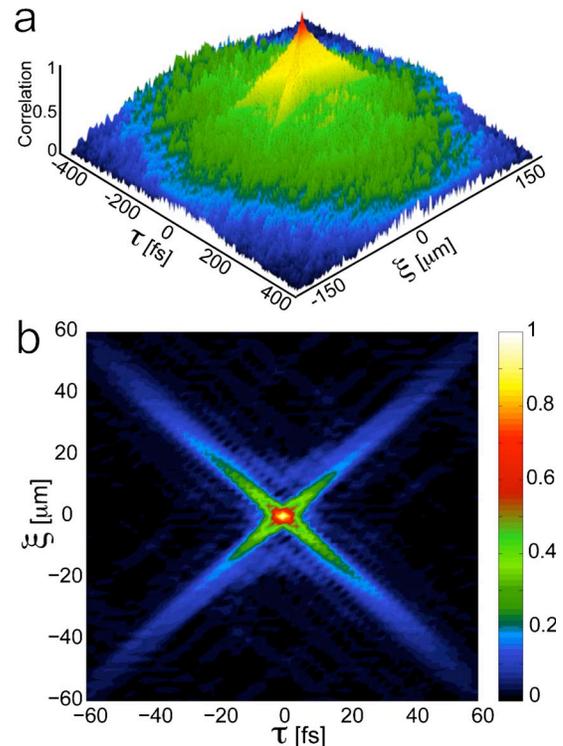
were smoothed out when taking the spectral average over the realizations.

Keeping in mind these considerations, we have analyzed, by using only single shot spectra, the shape of the radiation coherence for different phase-matching conditions, the latter reproduced by slightly tilting (maximum two degrees from degenerate configuration) the angle of the nonlinear crystal with respect to the pump direction. The angular distribution of the output parametric radiation follows the phase-matching curves of the crystal, in accordance with previous results [17,33]. The different recorded single-shot spectra together with the contour plots of their spatiotemporal Fourier transform are shown in Fig. 6. Note that, while the X-shaped structure is still present, slight differences from one correlation structure to another exist, following the change of shape of the radiation spectrum as a function of the crystal tilt angle.

The results presented in this section clearly indicate that the physical origin of X coherence in the near-field pattern relies on the conditions of energy and momentum conservation (phase-matching conditions), which in turn lead to a far-field spectrum characterized by chromatic and angular dispersion. As a matter of fact, the parametric amplification process is known to occur provided that a well-defined phase relationship between the pump and the down-converted fields is satisfied [43]. The coherence properties of the generated fields have to be those for which such phase relations are preserved during the propagation of the fields in the crystal. This leads to the spontaneous emergence of a particular field-mode geometry in the parametric wave-mixing process. The selection of the field-mode geometry occurs in such a
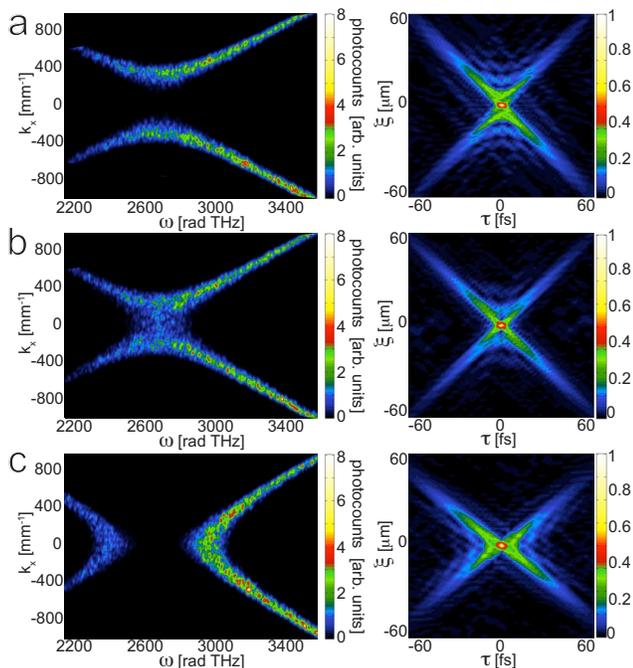
FIG. 6. (Color online) Single-shot spectra from BBO recorded for three different phase-matching conditions (crystal tuned out of degeneracy) (a) and relative contour plots of the bidimensional Fourier transform (b).

way that the phase relations between the interacting fields are preserved despite the presence of chromatic dispersion and diffraction effects. As a result, preferential amplification (i.e., maximum gain) occurs for the radiation modes whose phase relations can be statistically described by an *X*-shaped correlation (see Fig. 1). This is the subject of the next section (Sec. II C).

Finally note that, quite importantly, the characteristic *X*-shaped structure is also recovered in the analysis of higher-order correlation functions, e.g., in the signal-idler intensity cross-correlation. Indeed, preliminary numerical investigations indicate that, at the crystal output (i.e., in the near field), the signal field and the corresponding phase-conjugated idler field are not exactly correlated at the same time and at the same spatial point, but rather within an *X*-shaped spatiotemporal contour area [44].

C. Analogy with linear *X* waves

Coming back to our analysis of the field autocorrelation, it is worth pointing out that this does not permit us to characterize the exact mode structure of the generated field. Our study of the coherence in the full spatiotemporal domain is indeed based on a statistical approach, and the results obtained here only suggest that the superfluorescence radiation within the crystal may be statistically described as a "gas" of coherent states with a characteristic spatiotemporal skewed structure (see Fig. 1). As already mentioned in the previous section, this kind of radiation belongs to the family of conical waves—such as, for instance, *X* waves in normal dispersion—(for a review, see Ref. [45], and references

therein), and similar to the latter is characterized by an autocorrelation function that mixes space and time in a nonseparable way. It is interesting to recall that conical waves exhibit a very localized peak, in both transverse and longitudinal (temporal) coordinates, which propagates free from diffraction and dispersion, even in dispersive materials, for distances far exceeding those achievable with a conventional Gaussian-like beam, and that they are stationary modes of the linear propagation equation [28]. Here, from the analysis of the radiation autocorrelation function, only the statistical distribution of spatiotemporal modes may be pictured. In the following we would like to comment on the stationarity of these modes.

It can be shown that in the nonparaxial approach, the condition of stationarity of the intensity in some moving reference frame, requiring the axial propagation constant k_z to be a linear function of frequency [46], can be expressed in the form $k_z(\Omega) = (k_1 - \beta) + (k_1' - \alpha)\Omega$, where α and β are free parameters. Considering that $K = \sqrt{k_1^2(\omega) - k_{1,z}^2}$, a dispersion relation depending on these free parameters, can be derived for a nonparaxial description of wave modes in dispersive media. By adjusting opportunely the values of α and β, the dispersion relation curve can then be compared with the one describing the phase-matching process in the nonlinear medium under consideration. Note that Orlov and co-workers have demonstrated within a paraxial approximation approach that the creation of broadband localized fields inside the crystal of optical parametric generators is feasible [16]. In Fig. 7, we show for two different cases a qualitative agreement between a portion of phase-matching curve and the spatiotemporal spectrum of the stationary wave mode. We could imagine then that for each laser shot the superfluorescence radiation consists of a random distribution of "quasistationary" modes. In fact, because the characteristics of the angular dispersion set in by the phase-matching process are slightly different from that supporting a linear stationary mode, we are able to say that the autocorrelation function of the field is actually not fully stationary. As will be shown in Sec. III, also the nonlinear dynamics contributes to the imperfect stationarity of the correlation, the angular spectrum experiencing modification in its overall shape, along with the amplification. As a result, the autocorrelation progressively develops starfishlike arms during propagation, consistently with the fact that *X* waves are "long-range" objects.

D. Experimental results from a type-I LBO crystal

The aim of this section is to present the single-shot spatiotemporal spectrum of the parametric superfluorescence emitted by a type-I LBO crystal pumped by a 525 nm laser pulse, and the result of the bidimensional spatiotemporal Fourier transform applied to this spectrum. Because of the broad spectral range of the emitted radiation lying in this case from the red to far-infrared region, and because of the limited high detection efficiency range of the CCD (the latter having quantum efficiency going rapidly to zero for wavelengths greater than 1000 nm), only one portion of the spatiotemporal spectral structure could be measured. Nevertheless from symmetry considerations related to the energy and
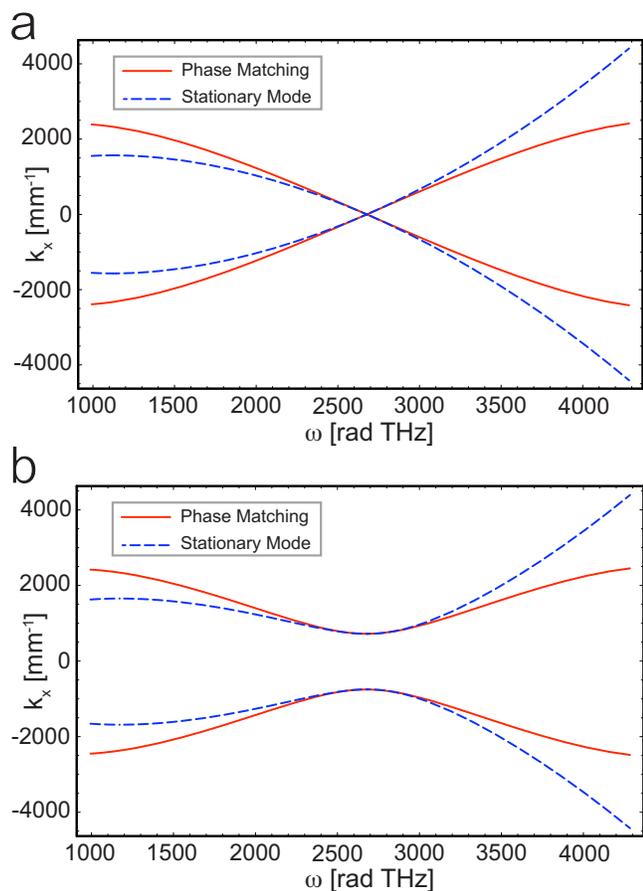
FIG. 7. (Color online) Comparison between phase-matching curve and spectrum of the nonlinear stationary mode of propagation, for two different phase-matching cases, associated with (a) $\alpha = 0$, $\beta = 0$ and (b) $\alpha = -0.0005 k_1'(\omega_0)$, $\beta = 45 \times 10^{-5} k_1'(\omega_0)$, respectively.

momentum conservation laws of the nonlinear process, we expect a symmetric structure around degeneracy, as for the case of the BBO radiation spectra. Figure 8 shows a single-shot spectrum retrieved in these conditions. The complete spectral curve has been obtained by duplicating, around the
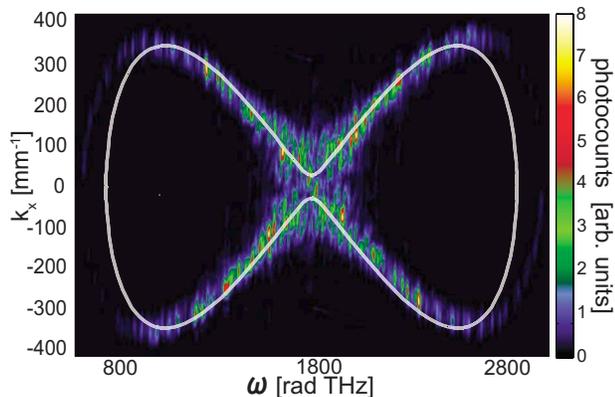

FIG. 8. (Color online) Single-shot spectrum of parametric down-conversion radiation generated by a type-I LBO crystal pumped at 527 nm and comparison with the theoretical phase-matching curve (white curve).
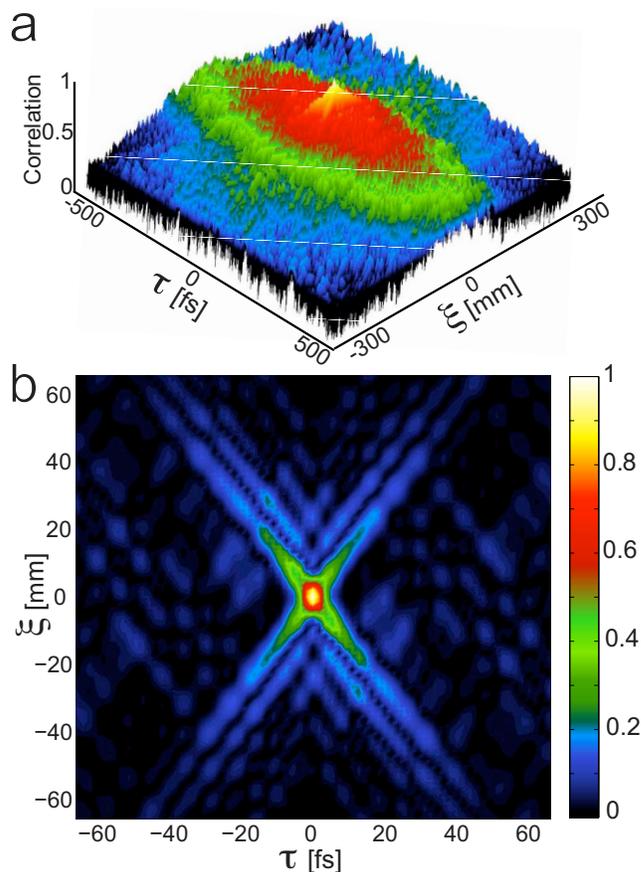

FIG. 9. (Color online) Bidimensional Fourier transform of the single shot spectrum from LBO (a), contour-plot representation (b).

degenerate frequency, the portion of spectrum effectively measured. The curvature of the X-spectrum arms leads to an "∞ shape," already observed in Ref. [32]. This peculiar feature will be discussed in the next section of the paper.

By applying the spatiotemporal Fourier transform of this spectrum we obtain the results presented in Figs. 9(a) and 9(b). Even in presence of a background, the X shape of the mutual coherence function is clearly visible through the contour plot representation shown in Fig. 9(b). The central peak dimensions are of the order of 8 ± 1 μm and 6 ± 2 fs.

III. THEORETICAL DESCRIPTION OF THE EMERGENCE OF X COHERENCE

Further insight into the mechanism underlying the emergence of X coherence may be obtained through the analysis of Maxwell's equations describing the propagation of the optical fields in the crystal [29]. Our aim here is to provide an extension of the brief theoretical treatment presented in Ref. [14]. Note that the whole theoretical treatment presented in this section is only relevant for the propagation of the fields within the quadratic nonlinear crystal, while the reshaping of X coherence during the propagation of the fields in air will be briefly discussed in the next section. Let us split the electric field amplitude into the fundamental and second harmonic components $E = \frac{1}{2}[E_1 \exp(-i\omega_1 t) + E_2 \exp(-i\omega_2 t)$

+c.c.], which allows one to derive the following coupled nonlinear equations governing the evolution of the corresponding envelopes $E_{1,2}(t,\vec{r})$

$$\frac{\partial^2 E_1}{\partial z^2} + \Delta_\perp E_1 + \int k^2(\Omega + \omega_1)\tilde{E}_1(\Omega,\vec{r})\exp(-i\Omega t)d\Omega$$

$$= -\chi^{(2)}\left(\frac{\omega_1}{c}\right)^2 E_2 E_1^*, \qquad (2)$$

$$\frac{\partial^2 E_1}{\partial z^2} + \Delta_\perp E_2 + \int k^2(\Omega + \omega_2)\tilde{E}_2(\Omega,\vec{r})\exp(-i\Omega t)d\Omega$$

$$= -2\chi^{(2)}\left(\frac{\omega_1}{c}\right)^2 E_1^2, \qquad (3)$$

where z denotes the longitudinal axis of propagation of the fields, $\vec{r}_\perp = (x,y)$ the transverse position vector, and $\Delta_\perp = \partial_x^2 + \partial_y^2$ the corresponding transverse Laplacian. The dispersion relation is $k(\omega) = \omega n(\omega)/c$, $n(\omega)$ being the refractive index at frequency ω, and $\tilde{E}_{1,2}(\Omega,\vec{r})$ refers to the temporal Fourier's transform of $E_{1,2}(t,\vec{r})$. We implicitly assumed in Eqs. (2) and (3) that axial emission occurs at degeneracy ($K=0$ for $\Omega=0$). Let us remark that these equations are valid beyond the usual paraxial and slowly varying envelope approximations. In the limit where the depletion of the pump wave may be neglected, the equation governing the evolution of the signal envelope $E_1 = A_1 \exp(ik_1 z)$ may readily be linearized to get

$$\frac{\partial^2 \hat{A}_1(\vec{K},\Omega)}{\partial z^2} + 2ik_1\frac{\partial \hat{A}_1(\vec{K},\Omega)}{\partial z} + [k^2(\omega_1 + \Omega) - k_1^2$$

$$- K^2]\hat{A}_1(\vec{K},\Omega) = -\sigma\hat{A}_1^*(-\vec{K},-\Omega), \qquad (4)$$

where

$$\hat{A}_1(\vec{K},\Omega,z) = \int dt \int d^2\vec{r}_\perp A_1(t,\vec{r}_\perp,z)\exp(-i\vec{K}\cdot\vec{r}_\perp)\exp(-i\Omega t) \qquad (5)$$

refers to the spatiotemporal Fourier's transform of the signal envelope at the propagation length z, and $\sigma = \chi^{(2)}\omega_1^2|E_2|/c^2$. By means of the Laplace transform $\hat{A}_1(\vec{K},\Omega,\gamma) = \int_0^\infty \hat{A}_1(\vec{K},\Omega,z)\exp(-\gamma z)dz$, the growth rate γ of the parametric instability is shown to satisfy the following dispersion relation:

$$\{(2k_1\mathcal{I})^4 - 2(2k_1\mathcal{I})^2[Q - (2k_1\gamma)^2]$$

$$+ [Q + (2k_1\gamma)^2]^2\}/[(2k_1\mathcal{I})^2 - Q] = 0 \qquad (6)$$

with $Q = [2k_1\mathcal{P} - K^2 + \gamma^2]^2 - \sigma^2$. The quantities $\mathcal{I} = \sum_{i=0}^\infty \Omega^{2i+1}k_1^{(2i+1)}/(2i+1)!$ and $\mathcal{P} = \sum_{i=1}^\infty \Omega^{2i}k_1^{(2i)}/(2i)!$, respectively, refer to the odd and even expansions of the wave vector $k(\omega_1 + \Omega) = \mathcal{P} + \mathcal{I}$ around ω_1. The explicit solutions to the dispersion relation (6) are extremely involved. It is worth noting, however, that the angular-spectrum of the radiation is relatively narrowband ($\Delta\theta \simeq 5° = 0.09$ rad $\ll \pi$ in Figs. 3, 6, and 8), so that physical insight may be obtained in the limit

of the paraxial approximation, where the parametric growth-rate γ takes the following simplified form:

$$\gamma(K,\Omega) = i\mathcal{I} + \sqrt{\sigma^2/4k_1^2 - (\mathcal{P} - K^2/2k_1)^2}. \qquad (7)$$

More precisely, in the framework of the paraxial approximation, one may derive the exact solution to the equation governing the evolution of $\hat{A}_1(\vec{K},\Omega,z)$ [Eq. (4) with $\partial_z^2\hat{A}_1 \equiv 0$]:

$$\hat{A}_1(\vec{K},\Omega,z) = U(\vec{K},\Omega)\hat{A}_1(\vec{K},\Omega,0) + V(\vec{K},\Omega)\hat{A}_1^*(-\vec{K},-\Omega,0), \qquad (8)$$

where

$$U(\vec{K},\Omega) = \exp(i\mathcal{I}z)\left[\cosh(\Gamma z) + i\frac{\Delta}{\Gamma}\sinh(\Gamma z)\right], \qquad (9)$$

$$V(\vec{K},\Omega) = \frac{i\sigma}{2k_1\Gamma}\exp(i\mathcal{I}z)\sinh(\Gamma z), \qquad (10)$$

with $\Delta = \mathcal{P} - K^2/2k_1$, $\Gamma = (\sigma^2/4k_1^2 - \Delta^2)^{1/2}$. Note that this solution is valid beyond the usual slowly varying envelope approximation [29]. The analytical solution (8)–(10) may be exploited to calculate the evolution of the spatiotemporal spectrum of the signal field during its propagation in the crystal

$$\langle S(K,\Omega,z)\rangle = \langle|\hat{A}_1|^2\rangle = \langle S(K,\Omega,z=0)\rangle\left[1 + \frac{2\sigma^2}{4k_1^2\Gamma^2}\sinh(\Gamma z)\right]. \qquad (11)$$

This expression reveals that the complex parameter Γ determines the nature of the parametric amplification process. Space-time frequencies for which Γ is real exhibit an exponential growth, while the others for which the parameter is imaginary will evolve in oscillatory fashion.

Let us first analyze the spectrum (11) within the slowly varying envelope approximation. The expansion of the wave vector $k(\omega_0 + \Omega)$ is thus truncated to the second order in $\mathcal{P}$, and the parametric growth rate reduces to $\gamma = [\sigma^2/4k_1^2 - (k_1''\Omega^2/2 - K^2/2k_1)^2]^{1/2}$ (note that $k_1'' \equiv k_1^{(2)}$). It becomes apparent from this expression that, depending on the sign of the dispersion parameter k_1'', two qualitatively different regimes of parametric amplification are found. In the anomalous dispersion regime ($k_1'' < 0$), $\gamma(K,\Omega)$ has a symmetric structure which reflects the symmetric role of space and time. Conversely, in normal dispersion ($k_1'' > 0$), $\gamma(K,\Omega)$ exhibits a hyperbolic structure, which means that the modes lying on the X-shaped spectrum are preferentially amplified in the parametric process, as previously anticipated through simple phase-matching considerations (see Sec. II A).

The corresponding evolution of the correlation function $C(\tau,\xi,z)$ is obtained by means of the spatiotemporal Fourier transform of $\langle S(K,\Omega,z)\rangle$ (see Sec. II B). It reveals that X coherence emerges progressively during the field propagation in the crystal, in a way that may remind the reader of the growth of starfish arms (see Fig. 10). This peculiar feature could be intuitively explained as follows. Let us consider one of the arms of the X spectrum, say, e.g., the right-tilted line
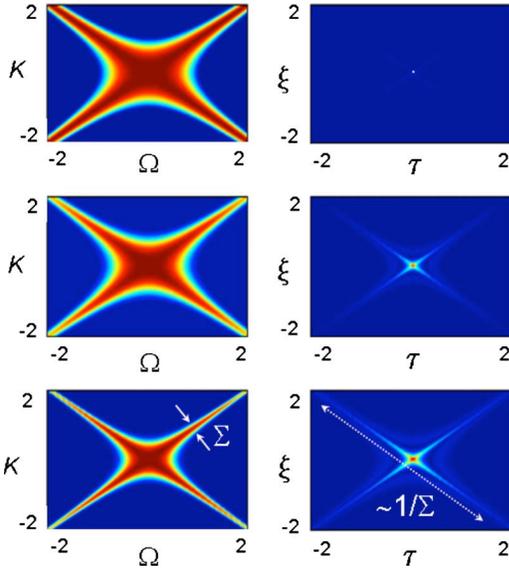
FIG. 10. (Color online) Left column: Evolution during the propagation z of the spatiotemporal spectrum $\langle \mathcal{S}(K,\Omega,z)\rangle$ obtained from Eq. (11). Right column: Corresponding evolution of the correlation function $\mathcal{C}(\xi,\tau,z)$ obtained from the spatiotemporal Fourier's transform of $\langle \mathcal{S}(K,\Omega,z)\rangle$. As the bandwidth Σ of the X spectrum gets narrower, the corresponding arms of the X correlation get longer. The three rows correspond, respectively, to $z=2L_{nl}$, $z=4L_{nl}$, $z=15L_{nl}$, with $L_{nl}=1/\sigma$. The variables τ and ξ (Ω and K) are in units of τ_0 and Λ_0 ($2\pi\tau_0^{-1}$ and $2\pi\Lambda_0^{-1}$), where $\tau_0=(L_{nl}k_1''/2)^{1/2}$ and $\Lambda_0=(L_{nl}/2k_1)^{1/2}$.

(or /) defined by the straight line $K=+\sqrt{k_1 k_1''}\,\Omega$. Let us note that Σ is the characteristic bandwidth of such a right-tilted line (see Fig. 10). Expanding $\gamma(K,\Omega)$ in the proximity of $K=+\sqrt{k_1 k_1''}\,\Omega$, the characteristic bandwidth is shown to evolve according to $\Sigma \propto (\sigma/z)^{1/2}/|K| \sim (\sigma/k_1 k_1'' z)^{1/2}/|\Omega|$. This means that due to the parametric amplification process [47,48], the characteristic width Σ of the right-tilted line gets narrower during the propagation of the field ($\Sigma \propto 1/z^{1/2}$). The corresponding length of the left-tilted line (or \) gets longer in the X-correlation function (see Fig. 10), as a result of the familiar property of the Fourier's transform. Accordingly, the signal field becomes self-correlated along two specific spatiotemporal trajectories $\tau=\pm\sqrt{k_1 k_1''}\,\xi$. Let us remark that in the limit in which dispersion (diffraction) dominates the interaction, i.e., k_1'' tends to infinity (zero), the arms of the X-correlation function get superposed and parallel to the temporal (spatial) axis. It is only in these two particular cases that the coherence properties of the generated field can be correctly described by the usual concepts of spatial and temporal coherence. In the general case of skewed coherence, the use of these usual concepts would lead to the conclusion that the field exhibits no coherence since it is neither spatial nor temporal.

Let us now study the influence of higher-order dispersion effects on the coherence properties of the generated signal field. According to the expression of the signal spectrum (11), maximum gain occurs for those spatiotemporal frequencies satisfying $\Delta(K,\Omega)=\mathcal{P}-K^2/2k_1=0$. The role of fourth-order dispersion may be analyzed by retaining the first
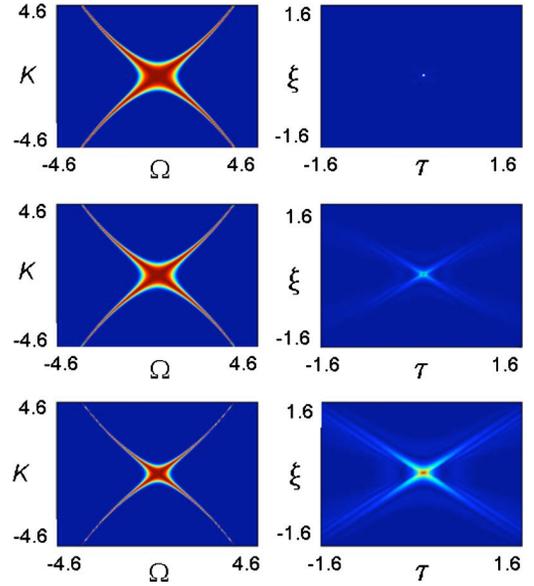

FIG. 11. (Color online) Same as in Fig. 10, but in the presence of positive fourth-order dispersion. The three rows correspond, respectively, to $z=2L_{nl}$, $z=4L_{nl}$, $z=15L_{nl}$ [$L_{nl}=1/\sigma$, $\tau_0=(L_{nl}k_1''/2)^{1/2}$, $\Lambda_0=(L_{nl}/2k_1)^{1/2}$, $k_1^{(4)}=+0.36k_1''^2 L_{nl}$].

two terms in the expansion of $\mathcal{P}(\Omega)$, which gives the following relationship between the spatial and temporal frequencies

$$K = \pm |\Omega|\sqrt{k_1 k_1^{(2)}(1 + k_1^{(4)}\Omega^2/12k_1^{(2)})}. \quad (12)$$

This expression reveals that fourth-order dispersion leads to a curvature in the arms of the X-shaped spectrum, as illustrated in Figs. 11 and 12. If $k_1^{(4)}$ is positive, both arms are inclined toward the K axis (Fig. 11), whereas they are in-
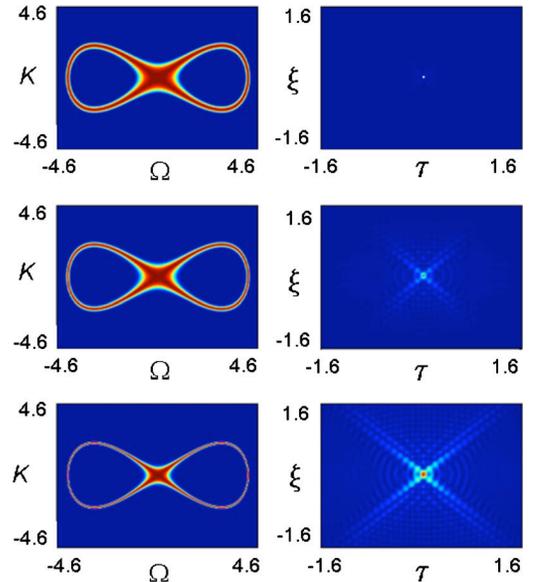

FIG. 12. (Color online) Same as in Fig. 10, but in the presence of negative fourth-order dispersion. The three rows correspond, respectively, to $z=2L_{nl}$, $z=4L_{nl}$, $z=15L_{nl}$ [$L_{nl}=1/\sigma$, $\tau_0=(L_{nl}k_1''/2)^{1/2}$, $\Lambda_0=(L_{nl}/2k_1)^{1/2}$, $k_1^{(4)}=-0.36k_1''^2 L_{nl}$].

clined toward the Ω axis for $k_1^{(4)}<0$ (Fig. 12). In this latter case, the curvature forms a closed loop at $\Omega_c = \pm\sqrt{12k_1^{(2)}/|k_1^{(4)}|}$, leading to an ∞-shaped spatiotemporal spectrum. As a result of this analysis it is found that fourth-order dispersion effects merely explain the origin of the ∞-shaped spectrum retrieved in the LBO experiment (Fig. 8), in which $k_1^{(4)}<0$ $(k_1^{(4)}=-1.05265\times10^{-13}$ ps$^4/\mu$m). Note, however, that the expression $\Omega_c=\pm\sqrt{12k_1^{(2)}/|k_1^{(4)}|}$ provides poor agreement with the corresponding value of Ω_c measured experimentally. Nevertheless, to reduce the discrepancy, one has just to include higher order dispersion effects in the expansion of $\mathcal{P}(\Omega)$ [including the six-order dispersion effect, one obtains $(\Omega_c-\Omega_c^{\mathrm{exp}})/\Omega_c^{\mathrm{exp}}\simeq7\%$]. Let us finally make the important point that, regardless of the sign of fourth-order dispersion, the spatiotemporal correlation function still exhibits an X-shaped structure, which is reminiscent of the coherence properties induced by second-order dispersion effects. The X-shaped spatiotemporal coherence then constitutes the natural state of coherence of parametrically amplified fields, beyond the standard slowly varying envelope approximation.

IV. YOUNG'S TWO-PINHOLE EXPERIMENT

The last step of this work is related to an interferometric measurement based on the well-known Young's two-pinhole experiment. This experiment was initially proposed in Ref. [15] to identify the coherence hidden in the spatiotemporal domain, and it was subsequently realized in Ref. [14]. Here we present a detailed description of the experiment, which provides an alternative experimental demonstration of the existence of X coherence. In order to perform this experiment, two pinholes have been realized by evaporating the aluminium surface of a metallic mirror. This was made by focusing on the mirror an intense green laser (527 nm) pulse by means of a microscopic objective. During this operation the mirror was mounted on a translation stage with micrometric movement in order to adjust the distance a between the two pinholes. The width of each pinhole ($d=5\pm0.5$ μm) and the distance between them ($a=30\pm4$ μm) have been quantitatively characterized by analyzing the standard Young's interference fringe pattern (visibility) obtained by using a cw green laser diode as the source. The interferometric measurement was then performed by sending the parametric down-conversion radiation emitted by the BBO crystal on the two-pinhole screen and by recording the diffraction pattern with the CCD camera. A scheme of the experimental setup is presented in Fig. 13. The latter shows in detail the configuration of the two-pinhole "screen." It consists of an aluminum surface (denoted by Al) evaporated on a 6 mm BK7 glass substrate. In front of the pinhole screen is placed a 0° high-reflectivity mirror (reflectivity > 99.9% at 352 nm) in order to remove the uv frequency components of the pump field. As already pointed out [14], the result of the experiment shows that rather than producing the usual single-peak fringe pattern [3], X coherence leads to a double-peak pattern (Fig. 14), where each peak arises from one arm of the X correlation [15]. In order
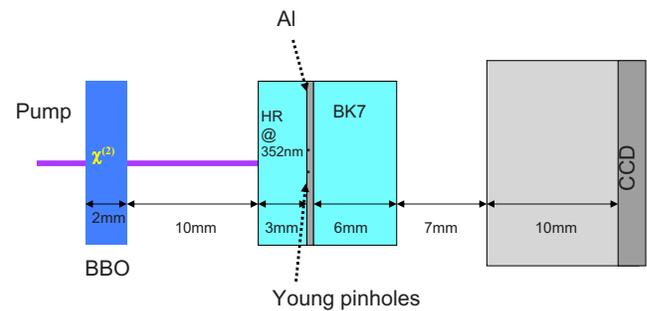

FIG. 13. (Color online) Scheme of the experimental setup used for Young's two-pinhole experiment

to emphasize the double-peak structure, an integrated profile of the recorded pattern has been obtained by binning the CCD pixels along the vertical axis. Indeed, the fringe visibility is given by the normalized correlation function $\mathcal{C}(\xi=a,\tau)$, in which ξ is fixed to the distance a between the pinholes and τ corresponds to the time delay between the two beams coming from the two pinholes [3]. The double-peak structure then reflects the ability of the field to interfere with a spatially shifted version of itself, provided it is delayed by appropriate times $\tau_\pm$, determined by the spatiotemporal trajectories $\tau_\pm\simeq\pm\sqrt{k_1k_1''}a$. These trajectories are those in which temporal dispersion and spatial diffraction compensate each other (see Sec. I). Note that the limited visibility of the fringes in Fig. 14 may be ascribed to the short time correlation ($\tau_c\simeq5$ fs), which is close to the optical cycle time and thus limits the spatial extension of the visibility pattern Δx to the fringe period i_0 ($\Delta x/i_0=c\tau_c/\lambda_1\simeq1$).

The positions of the peaks of the visibility pattern are related to the slope of the skewed lines of coherence in the space-time reference frame. We define θ_{tilt} as the tilt angle between the normal to the propagation axis ($\tau=0$) and the top right arm of $\mathcal{C}$. This is approximately given by 20° from a fit of Fig. 4(b). This value has to be compared with the angle of the skewed coherence line liable to form the visibility pattern reported in Fig. 14. The position of a visibility-peak x_m on the CCD screen plane is indeed related to the tilt-angle of the radiation arriving at the pinholes plane (13 mm behind the crystal output facet, see Fig. 13), denoted
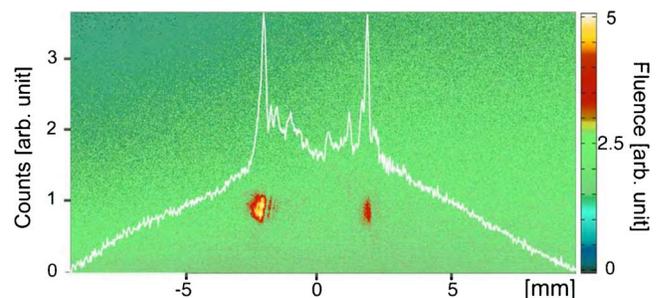

FIG. 14. (Color online) Experimental fringe pattern obtained by means of Young's interference experiment. The signal radiation is recorded on the CCD screen plane placed 23 mm behind the two-pinhole screen. The white curve is the integrated profile obtained after binning along the vertical pixels.

here by ϑ_{Young}, according to $\delta(x_m) = a/\tan(\vartheta_{\text{Young}})$, where $\delta(x_m)$ is the optical path difference between the two beams that emanate from the two pinholes and that arrive at x_m. The optical path difference has to be evaluated by taking into account that, before reaching the CCD screen, the radiation propagates through 6 mm of glass and 17 mm of air (see Fig. 13). From the experimental result and using optical refraction laws, one obtains $\vartheta_{\text{Young}} \cong 5°$. This value cannot be directly compared with the value of θ_{tilt} measured from the spatiotemporal coherence profile, but it is important to note that the propagation in air from the BBO crystal to the pinholes is expected to cause a sizable tilt reduction, resulting from finite beam size effect (see, e.g., Ref. [49]). Referring to Ref. [49], our calculations show that a tilt reduction from 20° to 5° should indeed be obtained in first approximation for 80 fs duration tilted pulses, having a full width at half maximum size of 70 μm. These values are in good agreement with the extension of the arms of the X-correlation function illustrated in Fig. 4(b). Accordingly, the positions of the peaks on the visibility pattern in Fig. 14 are consistent with those expected from the analysis of the correlation function measured experimentally. It is interesting to note that, if the pinholes were moved further away from the crystal (i.e., in the case of further propagation in air) the tilt of the radiation would tend to zero. We thus expect that the two arms of the X-wave field would tend toward almost plane-wave fronts. Accordingly, the two arms would give rise, separately, to lateral interference patterns, which would look similar to the usual white-light textbook fringe patterns. From the experimental point of view, it might be difficult to observe this phenomenon because of the low signal-to-noise ratio caused by the long propagation of the field in air.

We briefly mention that in order to better understand the result of this interference experiment, simplified numerical simulations have been carried out in order to compare the resulting interference pattern, for two different input field distributions. The first refers to a field distribution characterized by an amplitude given by a Bessel function of first order J_0 [50], which represents a monochromatic conical wave. The second refers to a stochastic distribution of several Bessel waves with amplitude J_0, each of them being characterized by a random global phase and a random position of its center with respect to the pinholes axis of symmetry. The interference pattern resulting from the second distribution (data not shown) indicates a slight reduction of the visibility of the central fringes, due to the fact that the modes contained in the stochastic distribution are not correlated. This is in agreement with the intuitive idea that X coherence leads to a double peak fringe pattern.

V. CONCLUSIONS

In this paper, we have presented detailed measurements of coherence of superfluorescence parametric radiation in the whole spatiotemporal domain, evidencing the skewed nature of the correlation retrieved. Application of the usual, purely spatial or temporal, coherence measurements would erroneously lead to the conclusion that the generated field is neither spatially nor temporally coherent. Such hidden coherence

has been identified thanks to the spectral diagnostic technique used, based on an imaging spectrometer and combined with the generalized form of the well-known theorem of Wiener-Kintchine. The X-shaped coherence function has been retrieved in this way for the superfluorescence emitted in perfect phase-matching conditions at degeneracy, from a type-I BBO crystal, and has been compared with the bidimensional spatiotemporal Fourier transform applied to a single-shot spectrum. Having observed that the angular features and shape of the structure emerging from this analysis reflects those of the effective spatiotemporal correlation function of the radiation well, the analysis has been further extended, by using single-shot spectral measurements, to other configurations with the crystal angle tilted with respect to the pump direction, so as to fulfill different phase-matching conditions (noncollinear emission at degeneracy). For the radiation generated by a type-I LBO crystal, the "∞-shaped" phase-matching curve has been clearly evidenced and confirmed by the theoretical analysis of Maxwell equations, and the skewed features of the field correlation has been revealed also in that case. The realization of Young's interference experiment has corroborated the existence of X coherence. A theoretical analysis of the equations governing light propagation in the crystal has also provided insight into the mechanism underlying the emergence of X coherence. As a result, X-shaped spatiotemporal coherence appears as the natural state of coherence of superfluorescence light, beyond the standard slowly varying approximation. The generated radiation may be statistically described as a random superposition ("gas") of modes. These are characterized by a skewed spatiotemporal structure not describable within a separable approach in space and time, similarly to X waves, which are known as the stationary modes of the linear and nonlinear process [28]. Clearly, the above interpretation does not give a precise deterministic picture of the near field distribution at the crystal output and for each laser shot nor does it allow us to say that the modes of the parametric down-converted radiation are really X-type modes, but simply suggests how these can be visualized as extended over pieces or portions of skewed spatiotemporal correlation. We have also noted that the spatiotemporal correlation can be considered to be quasistationary, the phase-matching curve of the nonlinear crystal partially coinciding with the spectrum of the stationary conical wave mode in a dispersive material. We may also see the parametric down-conversion process as similar to, in some sense, the stochastic counterpart of the deterministic generation of X waves in the phase-mismatched second-harmonic generation nonlinear process [19–23]. Finally, note that in addition to the emergence of the long-range skewed tails of the correlation, an interesting result of this work is also given by the narrowness of the central peak of the correlation function of the radiation, both in space and in time, thus approaching the single-cycle optical pulse length and duration. This opens new perspectives for the attempt of generation, in parametric amplification processes, of a single ultrashort coherent single-cycled localized X wave; work is in progress in this direction.

Our study also generalizes the concept of coherence in any field where partially coherent states cannot be described by means of the standard definitions of spatial and temporal

coherence. Let us stress then the general relevance of *X* coherence by emphasizing that it constitutes the natural state of coherence for all nonlinear systems whose governing equations exhibit a space-time hyperbolic structure, as discussed above through Eq. (7). *X* coherence is thus expected to arise in any multidimensional optical system involving nonlinear wave propagation in normal dispersion. A typical example is the modulational instability of plane waves propagating in cubic $\chi^{(3)}$ nonlinear Kerr media [51]. In complete analogy with the present work, we have verified that *X* coherence emerges spontaneously in Kerr media in the modulational amplified noise fluctuations (data not shown). This is also what implicitly emerged in Ref. [52], where a numerical analysis of the amplification gain profiles in Kerr media has been made by seeding the material with a background white noise, and showing a specklelike *X*-shaped pattern in the spatiotemporal spectrum.

Note that space-time skewed coherence does not necessarily require radial symmetry in the phase-matching configuration. It is indeed sufficient to consider a noncollinear, planar interaction geometry. For instance, in the case of the standard process of four-wave mixing supported by a cubic nonlinearity, in which two noncollinear pump waves parametrically amplify two daughter waves from noise fluctuations [29], coherence emerges along those skewed spatiotemporal trajectories where spatial walk-off and temporal group-velocity difference compensate each other [15], in the same way that *X* coherence emerges along skewed lines where diffraction compensates chromatic dispersion. Four-wave mixing is indeed a very general process; it is known to play a key role not only in optics but also in such diverse fields as plasma [53], acoustic [54], water [55], and matter waves [2,56]. Considering specifically the process of parametric four-wave mixing in Bose-Einstein condensates [2,56], we may reasonably infer the formation of long-range phase coherence (condensation) along specific spatiotemporal lines. This feature might be revealed by means of (Young's) double-slit interference experiments [57]. However, following the spectral technique reported here, an alternative, simpler approach would consist of detecting correlation directly in the momentum distribution (spectrum) of the expanded matter wave.

Finally, we point out the natural importance that *X* coherence may have in the context of quantum optics. For instance, one may reasonably expect that the *X*-shaped spectrum characterizing the superfluorescence radiation emitted in high-gain parametric down-conversion, as well as the double-peak fringe pattern, would be similarly obtained if the acquisition were performed in the parametric fluorescence regime, i.e., photon-by-photon. This implies that each individual photon would be characterized by an *X*-shaped space-time correlation. An experiment in low-gain regime is also the topic of future work.

[1] J. F. Annett, *Superconductivity, Superfluids, and Condensates* (Oxford University Press, Oxford, 2004).

[2] P. Meystre, *Atom Optics* (Springer Verlag, New York, 2001).

[3] L. Mandel and E. Wolf, *Optical Coherence and Quantum Optics* (Cambridge University Press, New York, 1995).

[4] J. W. Goodman, *Statistical Optics* (Wiley-Interscience, New York, 1985).

[5] U. Frisch, *Turbulence: The Legacy of A. N. Kolmogorov* (Cambridge University Press, New York, 1995).

[6] J. Pokorny and T.-M. Wu, *Biophysical Aspects of Coherence and Biological Order* (Springer-Verlag, Telos, 1998).

[7] E. Wolf, Proc. R. Soc. London **230**, 246 (1955).

[8] R. J. Glauber, Phys. Rev. **130**, 2529 (1963).

[9] P. Hariharan, *Optical Interferometry*, 2nd ed. (Elsevier, Amsterdam, 2003).

[10] M. V. Lebedev, A. I. Filin, and O. V. Misochko, Meas. Sci. Technol. **12**, 736 (2001).

[11] R. Giordano, F. Mallamace, N. Micali, F. Wanderlingh, G. Baldini, and S. Doglia, Phys. Rev. A **28**, 3581 (1983).

[12] J. H. Scofield, J. V. Mantese, and W. W. Webb, Phys. Rev. B **34**, 723 (1986).

[13] V. Degiorgio, R. Piazza, and R. B. Jones, Phys. Rev. E **52**, 2707 (1995).

[14] O. Jedrkiewicz, A. Picozzi, M. Clerici, D. Faccio, and P. Di Trapani, Phys. Rev. Lett. **97**, 243903 (2006).

[15] A. Picozzi and M. Haelterman, Phys. Rev. Lett. **88**, 083901 (2002).

[16] S. Orlov, A. Piskarskas, and A. Stabinis, Opt. Lett. **27**, 2103 (2002).

[17] R. Butkus, S. Orlov, A. Piskarskas, V. Smilgevicius, and A. Stabinis, Opt. Commun. **244**, 411 (2005).

[18] S. Trillo, C. Conti, P. Di Trapani, O. Jedrkiewicz, J. Trull, G. Valiulis, and G. Bellanca, Opt. Lett. **27**, 1451 (2002).

[19] C. Conti, S. Trillo, P. Di Trapani, G. Valiulis, A. Piskarskas, O. Jedrkiewicz, and J. Trull, Phys. Rev. Lett. **90**, 170406 (2003).

[20] P. Di Trapani, G. Valiulis, A. Piskarskas, O. Jedrkiewicz, J. Trull, C. Conti, and S. Trillo, Phys. Rev. Lett. **91**, 093904 (2003).

[21] M. Kolesik, E. M. Wright, and J. V. Moloney, Phys. Rev. Lett. **92**, 253901 (2004).

[22] D. Faccio, M. A. Porras, A. Dubietis, F. Bragheri, A. Couairon, and Paolo Di Trapani, Phys. Rev. Lett. **96**, 193901 (2006).

[23] C. Conti and S. Trillo, Phys. Rev. Lett. **92**, 120404 (2004).

[24] M. A. Porras, S. Trillo, C. Conti, and P. Di Trapani, Opt. Lett. **28**, 1090 (2003).

[25] D. Faccio, P. Di Trapani, S. Minardi, A. Bramati, F. Bragheri, C. Liberale, V. Degiorgio, A. Dubietis, and A. Matijosius, J. Opt. Soc. Am. B **22**, 862 (2005).

[26] M. A. Porras, G. Valiulis, and P. Di Trapani, Phys. Rev. E **68**, 016613 (2003).

[27] C. Conti, eprint arXiv.org:quant-ph/0309069.

[28] M. A. Porras and P. Di Trapani, Phys. Rev. E **69**, 066606 (2004).

[29] R. W. Boyd, *Nonlinear Optics* (Academic Press, New York, 2002).

[30] T. G. Giallorenzi and C. L. Tang, Phys. Rev. **166**, 225 (1968).

[31] E. Lantz, L. Han, and A. Lacourt, Opt. Commun. **97**, 245 (1993).

[32] A. Berzanskis, W. Chinaglia, L. A. Lugiato, K.-H. Feller, and P. Di Trapani, Phys. Rev. A **60**, 1626 (1999).

[33] F. Devaux and E. Lantz, Eur. Phys. J. D **8**, 117 (2000).

[34] J. P. Budin, B. Godard, and J. Ducuing, IEEE J. Quantum Electron. **4**, 831 (1968).

[35] F. Devaux and E. Lantz, J. Opt. Soc. Am. B **12**, 2245 (1995).

[36] D. Faccio, M. A. Porras, A. Dubietis, G. Tamosauskas, E. Kucinskas Couairon, and P. Di Trapani, Opt. Commun. **265**, 672 (2006).

[37] D. Faccio, A. Averchi, A. Dubietis, P. Polesana, A. Piskarskas, A. Couairon, and P. Di Trapani, Opt. Lett. **32**, 184 (2007).

[38] J. Durnin, J. J. Miceli, and J. H. Eberly, Phys. Rev. Lett. **58**, 1499 (1987).

[39] E. Lantz and F. Devaux, Eur. Phys. J. D **17**, 93 (2001).

[40] E. Brambilla, A. Gatti, M. Bache, and L. A. Lugiato, Phys. Rev. A **69**, 023802 (2004).

[41] O. Jedrkiewicz, Y.-K. Jiang, E. Brambilla, A. Gatti, M. Bache, L. A. Lugiato, and P. Di Trapani, Phys. Rev. Lett. **93**, 243601 (2004).

[42] O. Jedrkiewicz, E. Brambilla, M. Bache, A. Gatti, L. A. Lu-giato, and P. Di Trapani, J. Mod. Opt. **53**, 575 (2006).

[43] A. Yariv, *Quantum Electronics*, 3rd ed. (Wiley, New York, 1989).

[44] A. Gatti and E. Brambilla (unpublished).

[45] A. Dubietis, G. Valiulis, and A. Varanavicius, Lith. J. Phys. **46**, 7 (2006).

[46] H. Sonajalg and P. Saari, Opt. Lett. **21**, 1162 (1996).

[47] A. Picozzi and M. Haelterman, Phys. Rev. E **63**, 056611 (2001).

[48] A. Picozzi and P. Aschieri, Phys. Rev. E **72**, 046606 (2005).

[49] O. Martinez, Opt. Commun. **59**, 229 (1986).

[50] M. Abramovitz and I. Stegun, *Handbook of Mathematical Functions with Formulas, Graphs, and Mathematical Tables* (Dover, New York, 1964).

[51] L. W. Liou, X. D. Cao, C. J. McKinstrie, and G. P. Agrawal, Phys. Rev. A **46**, 4202 (1992); G. G. Luther *et al.*, Opt. Lett. **19**, 789 (1994).

[52] D. Faccio, A. Averchi, A. Couairon, A. Dubietis, R. Piskars-kas, A. Matijosius, F. Bragheri, M. A. Porras, A. Piskarskas, and P. Di Trapani, Phys. Rev. E **74**, 047603 (2006).

[53] J. Weiland and H. Wilhelmsson, *Coherent Nonlinear Interaction of Waves in Plasmas* (Pergamon, Oxford, 1977).

[54] M. F. Hamilton and D. T. Blackstock, *Nonlinear Acoustics* (Academic Press, New York, 1998), Chap. 8, p. 14.

[55] E. Infeld and G. Rowlands, *Nonlinear Waves, Solitons and Chaos* (Cambridge University Press, Cambridge, 1992).

[56] L. Deng *et al.*, Nature (London) **398**, 218 (1999).

[57] I. Bloch *et al.*, Nature (London) **403**, 166 (2000).